ACS OMEGA

Open Access

http://pubs.acs.org/journal/acsodf

Article

Revealing Local Structure of Angiotensin Receptor-Neprilysin Inhibitor (S086) Drug Cocrystal by Linear and Nonlinear Infrared Spectroscopies

Wenjie Xu,[‖] Haiyan Xu,[‖] Jie Yan, Song Li, Pengyun Yu, Juan Zhao, Fan Yang, and Jianping Wang*

Cite This: *ACS Omega* 2024, 9, 49683−49691

Read Online

ACCESS | Metrics & More | Article Recommendations | Supporting Information

ABSTRACT: Structurally knowing the active sites of a drug is important for understanding its therapeutic functions. S086 is a novel angiotensin receptor-neprilysin inhibitor that consists of the molecular moieties of EXP3174 (the active metabolite of the angiotensin receptor blocker losartan) and sacubitril (a neprilysin inhibitor prodrug) in a 1:1 molar ratio. There are two forms of cocrystals of S086, namely, *ξ*-crystal and *α*-crystal, which were formed both via intermolecular coordination bonding to calcium ions, with the aid of internal water. The binding state of multiple carboxyl anions (COO^-) to Ca^{2+} of EXP3174 and sacubitril was examined in this study using infrared (IR) absorption spectroscopy, in which the asymmetric stretching (*as*) and symmetric stretching (*ss*) modes of the COO^- groups were used as IR probes. Ultrafast two-dimensional (2D) IR spectroscopy was utilized for spectrally assigning the origin of multiple COO^- groups by the presence or absence of interchromophore vibrational coupling. Key structural variation between the two crystal forms was found: in the unit cell of *ξ*-crystal, the ratio of "bridging" and "bidentate" types of COO^- binding to Ca^{2+} for four EXP3174 molecules is 2:2, while the ratio is predicted to be 3:1 in the case of *α*-crystal. However, in both crystals, four sacubitril molecules are believed to similarly form a "trident" type of COO^- binding to Ca^{2+}. Our study demonstrates that linear and nonlinear IR spectroscopies can be used to characterize local crystal structures of drugs and reveal subtle difference between similar crystal structures.

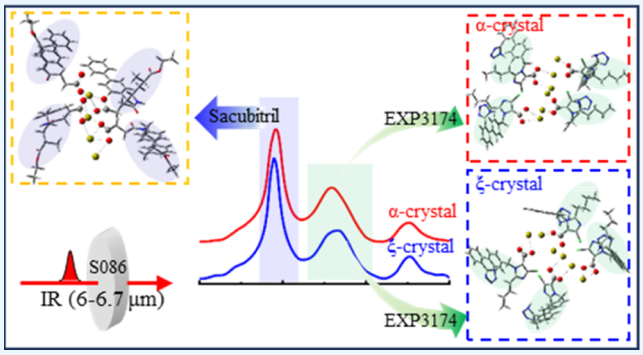

1. INTRODUCTION

Hypertension is well known as a chronic disease that is characterized by elevated systemic arterial pressure.[1,2] It is considered to be one of the major preventable risk factors for premature death and disability worldwide. It can also cause many complications and secondary diseases.[3] Heart failure (HF) is well accepted as a major complication in hypertensive patients.[4] Angiotensin receptor-NEP inhibitor (ARNI)[5,6] is composed of Angiotensin II receptor blocker (ARB)[7,8] and Neprilysin inhibitor (NEPi),[9,10] which is known to be effective in treating HF,[11] with superior effect than ACEI[12] and ARB.[13,14] Angiotensin receptor-neprilysin inhibitor (ARNI) is also approved as a new antihypertensive drug in Japan and China, which has been demonstrated to reduce office blood pressure and 24 h blood pressure.[15,16]

The first class of ARNI drugs was sacubitril valsartan sodium tablets (LCZ696), which consists of *N*-Valeryl-*N*-[2′-(1H-tetrazol-5-yl)biphenyl-4-ylmethyl]-L-valine (valsartan), 4-(((2*S*,4*R*)-1-((1,1′-biphenyl)-4-yl)-5-ethoxy-4-methyl-5-oxopentan-2-yl)amino)-4-oxobutanoic acid (sacubitril, AHU377), Na^+, and water in a ratio of 1:1:3:2.5. Clinical trials have shown that LCZ696 was effective and had no notable side effect.[11,13,14] In addition, a new amorphous drug was proposed by An et al. to enhance the stability of LCZ696, in which the molar ratio of sacubitril, valsartan, and calcium ion is 1:1:0.5.[17] Sacubitril allisartan calcium tablets (S086) were developed as a new type of eutectic combination composed of ARB and NEPi in the molar ratio of 1:1, and Ca^{2+} and hydrate.[3] It is expected to be a new and effective ARNI. The NEPi component in both LCZ696 and S086 is AHU377, which is metabolized by the enzymatic cleavage of its ethyl ester to the enkephalinase-inhibitory metabolite LBQ657.[18,19] Different from LCZ696, the ARB component in S086 is 2-butyl-4-chloro-1-[[2′-(1H-tetrazol-5-yl)[1,1′-biphenyl]-4-yl]methyl]-1H-imidazole-5-carboxylic acid (named as losartan carboxylic acid, allisartan, or EXP3174), and the latter is also known to be the first generation of ARB.[20] As a higher potency ARB in S086 than valsartan in LCZ696, EXP3174 may have a longer half time to achieve 24 h blood pressure control.[21] It is expected that S086

Received: August 27, 2024
Revised: November 3, 2024
Accepted: November 27, 2024
Published: December 4, 2024

Scheme 1. Chemical Composition of S086[a]

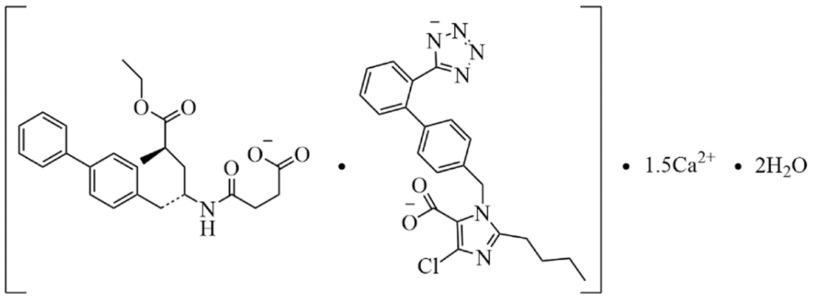

[a]From Left to Right: Sacubitril, EXP3174, Calcium Ion, and Water, with Molar Ratio = 1:1:1.5:2.

will be similarly effective as LCZ696 in treating chronic heart failure.[22]

Drug−drug cocrystals are usually assembled by two or more different drug molecules in the desired molar ratio via intermolecular interactions such as coordinate valence, $\pi-\pi$ stacking, hydrogen bonding, and van der Waals forces.[23] Drug−drug cocrystals are known to exhibit certain clinical advantages, which include enhanced physicochemical properties and new synergistic effects, as well as reduced expenses required for formulation and marketing of two individual drug products.[23] Therefore, it is critical to gain detailed structural insights into the drug−drug cocrystals.

S086 is a good example of a drug−drug cocrystal, which may exist in two different cocrystal forms with the same stoichiometry of EXP3174 and sacubitril, denoted here as α- and ξ-crystal forms.[24,25] Recently, this drug has been studied in clinical trials.[3,21,22] It is believed that the α- and ξ-crystal forms are structurally different, but the detailed differences are not known.

Classically linear infrared (IR, FTIR) spectroscopy is a very sensitive structural tool for studying structures of molecules and molecular complexes in solution, in solid (including crystal), as well as at interfaces.[26−31] Key chemical groups in a molecular complex can be characterized in IR spectroscopy in terms of vibrational frequency, intensity, and spectral line width and then used as vibrational parameters for understanding the local structures of the chemical groups. Ultrafast two-dimensional infrared (2D IR) spectroscopy developed two decades ago has been known to be able to reveal more vibrational parameters that are not available from conventional linear IR spectroscopy, including vibrational couplings among anharmonic vibrational modes, and vibrational energy transfer dynamics in a given molecular complex,[32−40] all of these parameters are useful in understanding the structure of the molecular complex. However, 2D IR application in the structural characterization of drug−drug cocrystals, to the best of our knowledge, has not been reported.

This study focuses on illustrating the interaction of calcium ions with the two molecular moieties in the two crystal forms of S086, with the aim of understanding the local structure of the α-crystal form, on the basis of the known unit-cell structure of the ξ-crystal form. Understanding such a local structural feature is critical to understand the structural stability, solubility, dissolving rate, and biological activities of S086. In particular, the binding states of multiple carboxyl groups (COO^-) that are key ligands of multiple Ca^{2+} ions in the two cocrystals of S086 are examined in detail. The asymmetric stretching (*as*) and symmetric stretching (*ss*) modes of a COO^- group are known to be structurally sensitive to molecular complexes containing carboxylates in solutions, in solids, and even at interfaces. Nakmoto[41] proposed that the frequency difference between the *as* and *ss* modes of the COO^- group can be used to determine the binding types between the COO^- group and metal cations. Deacon and Phillips[42] examined IR data of more than 70 metal carboxylates and proposed a general rule for determining the binding types of the COO^- group and metal cations, which were useful for the IR studies of drug−drug cocrystals in this study.

2. MATERIALS AND METHODS

2.1. Materials. All chemicals were obtained from commercial sources and were used without further purification. Two forms of sacubitril allisartan calcium complex (S086) cocrystals, namely, ξ- and α-crystal forms, consisting of sacubitril, EXP3174, and calcium cations were prepared. In both ξ- and α-crystal forms of S086, the molar ratio of sacubitril, EXP3174, calcium ion, and water is 1:1:1.5:2, whose chemical composition is shown in Scheme 1.

2.1.1. α-Crystal. First, sacubitril calcium (2 g, 4.5% moisture content) and isopropyl acetate (2.1 g) were added to a proper reaction flask, the temperature of which was controlled at 0−30 °C. A dilute hydrochloric acid solution [hydrochloric acid (0.9 g)/water (3.8 mL)] was then added slowly into the flask. The reactants were allowed to react at 20−30 °C for 1−2 h upon stirring. After the reaction solution became transparent, phase separation was carried out to discard the aqueous phase and collect the organic phase at 40−50 °C, resulting in sacubitril as an oily substance. Acetone (3.2 g) and EXP3174 (1.92 g, moisture content = 7.6%) were added to the oily substance, followed by stirring. Calcium hydroxide (0.47 g) and water (0.8 mL) were then added to the solution, stirring for 10−15 min and filter, followed by heating to 40−50 °C, and allowing reaction for 4 h. Under a nitrogen environment, the solid product was filtered and dried at 40−50 °C under vacuum for more than 12 h, giving rise to sacubitril allisartan calcium complex in the α-crystal form. The chemical purity of the α-crystal was determined to be 99.8%.

2.1.2. ξ-Crystal. The α-crystal form of sacubitril allisartan calcium complex (4 g), dichloromethane (160 mL), and water (0.04 mL) were added into a reaction flask, whose temperature was set to 20−30 °C. After stirring for more than 20 h, crystallization was completed, followed by filtration and washing with 2.0 g dichloromethane. The solid product was dried under vacuum conditions at 40−50 °C for more than 8 h. This yielded the ξ-crystal form of S086, whose crystal structure has been well determined by microcrystal electron diffraction (MicroED, see below). The chemical purity of the ξ-crystal was determined to be 99.8%.

https://doi.org/10.1021/acsomega.4c07887
ACS Omega 2024, 9, 49683−49691

2.1.3. Sacubitril Monomer. Sacubitril calcium was added to hydrochloric acid (pH ≈ 2.7) and then concentrated by organic phase (acetic acid isopropyl ester) to prepare the sacubitril monomer.

2.1.4. EXP3174 Monomer. After adding deionized water (250 mL) and potassium permanganate (0.25 mol) to a three-necked flask and stirring for 15 min, tetrabutylammonium chloride (0.30 mL) was added and the reaction mixture was stirred for 30 min. Subsequently, pyridine (100 mL) and acetone (650 mL) were added to the mixed solution, which was continuously stirred for 30 min and then heated to 40 °C. Losartan (0.1 mol) was added to the above mixed solution, which was heated continuously at 50 °C for 1 h. A 30% formaldehyde solution (200 mL) was slowly added to the reaction mixture, which was heated until a brown precipitate was formed. The reaction product was washed to colorless using a NaOH (1.0 M) solution and concentrated. HCI (6 M) solution was added to the concentrate to lower the pH (pH ≈ 2.0), and a white precipitate was formed. The white precipitate was filtered, washed, dried, and then recrystallized in 2-propanol to form a white EXP3174 solid.

2.2. Infrared Spectroscopic Measurement. Transmittance infrared spectral measurements were performed using a commercial Fourier transform infrared (FTIR) spectrometer (Nicolet 6700, Thermo Fisher) that is equipped with a liquid nitrogen-cooled mercury−cadmium−telluride (MCT) detector. Ambient CO_2 and H_2O moistures were removed by purging the FTIR sample chamber using dry air. Sample solutions of the α-crystal form in acetone (preferred), the ξ-crystal form in CH_2Cl_2 (preferred), sacubitril monomer, and sacubitril and EXP3174 mixture in acetone or CH_2Cl_2 were encased into two 2 mm thick CaF_2 windows separated by 30 μm Teflon spacer and housed in a stainless-steel IR sample-cell holder. Attenuated total reflection (ATR) IR spectra of EXP3174 power were also measured by Nicolet iS5 (Thermo Fisher). Each IR spectrum was accumulated over 64 scans at 1 cm^{-1} spectral resolution at room temperature (22 °C).

Ultrafast 2D IR spectroscopy was used to characterize the local structures and dynamics of S086 cocrystals. The experiments were performed in a pump−probe 2D IR geometry based on the IR pulse shaping method.[43] The system was driven by a Ti-sapphire laser amplifier with a center wavelength at 800 nm, energy of 3 mJ, pulse width of 25 fs, and repetition rate at 1 kHz, followed by an optical parametric amplifier and a difference frequency generator to produce the needed mid-infrared pulse. The delay time of two pump pulses (t) is scanned at a fixed waiting time (T_w) for a range of detection frequency ω_t so as to produce a time−frequency hybrid interferogram.[44] FT and inverse FT of obtained nonlinear IR signals from a given sample, acquired using an IR monochromator and MCT array detector, were post-performed to yield a 2D IR spectrum. Intramolecularly coupled vibrational modes were identified by 2D IR cross peaks at early T_w.

2.3. Diffraction Measurement. X-ray powder diffraction (XRD) of both α- and ξ-crystal forms of S086 was measured, whose diffraction intensity was recorded at 293 K on an Empyrean/Bragg−BrentanoHD diffractometer (Cu−Kα, λ = 1.54056 Å). MicroED (microcrystal electron diffraction) data set of the ξ-crystal form was collected using a JEOL 2100Plus transmission electron microscope (200 kV) equipped with a MerlinEM-4S camera, whose structure will be reported in a separate work and will be deposited to CCDC crystal library (pre-CCDC ID 2277834).

2.4. Quantum Chemistry Calculation. Quantum chemistry calculations were performed using density functional theory (DFT) at the level of B3LYP using Gaussian.[45] First, deuterated acetic acid (CD_3COO^-) was used to model the interaction between carboxylic acid and calcium ions at different binding geometries. Here, deuterated acetic acid is used to avoid the overlap between a rocking mode of CH_3 and the symmetric stretching mode of COO^-. Structural optimization and harmonic infrared vibrational frequency calculation were carried out in CH_2Cl_2 and DMSO using an implicit solvent model (polarizable continuum model).[46,47] The def2-tzvp basis set with Grimme dispersion correction was used.[48] Dependence of the asymmetric and symmetric COO^- stretching frequencies on the OCO bond angle and C═O bond length was examined. In addition, geometric optimization was also carried out for EXP3174 at the level of B3LYP with the 6-31+G** basis set,[49] from which the bond angle of the COO^- group was obtained.

3. RESULTS AND DISCUSSION

3.1. ξ-Crystal and α-Crystal Forms and Their IR Spectra. As shown in Scheme 1, there are four sacubitril molecules, four EXP3174 molecules, and six calcium ions in S086. The XRD spectra of ξ-crystal and α-crystal forms are shown in Figure S1a and S1b of the Supporting Information (SI). As can be seen, ξ-crystal appears to have sharper XRD peaks than α-crystal, indicating a better crystal structure in the former. Figure S2 of SI shows the structure of a unit cell of the ξ-crystal form of S086 derived from MicroED, indicating four sacubitril molecules are in a "trident" binding state with Ca^{2+}, and two EXP3174 molecules are in "bridging" binding state and two are in a "bidentate" binding state with Ca^{2+}. There are six total Ca^{2+} ions. These types of binding are defined for the interaction between the COO^- group and Ca^{2+} (see more details in Section 3.2). The MicroED results also show that for the ξ-crystal, it requires 12 positive ions (i.e., 6 Ca^{2+} ions) to balance totally 12 negative charges by four sacubitril molecules and four EXP3174.

To illustrate the local structure details of the α-crystal form of S086, the FTIR spectra of the two crystal forms are compared. The results are shown in Figure 1 in the region of carboxylic stretching mode and amide-I mode (mainly the C═O stretch of the −CONH− group) since the COO^- and amide groups are known to be coordinated with six Ca^{2+} ions in the ξ-crystal form (Figure S2a of SI).

First, Figure 1a shows an IR spectrum of the ξ-crystal form in CH_2Cl_2, which is area-normalized in the spectral range of 1500−1650 cm^{-1}. Its Voigt fitting results are listed in Table S4 of SI. Four relatively strong IR absorption peaks and one weak IR peak are observed. A single peak at 1544.9 cm^{-1} is assigned to the asymmetric stretching mode of carboxylic acid in sacubitril because in the 2D IR spectrum (Figure S3b of SI) this mode intramolecularly couples with the amide-I mode that is assigned to the 1626.6 cm^{-1} peak of Figure 1a. Here, according to Figure S2 of SI, the amide group mode is also coordinated to a Ca^{2+} ion. Second, two peaks are obtained at 1576.0 and 1585.2 cm^{-1} with an area ratio of ca. 1:1 by fitting. These two peaks can be assigned to the asymmetric stretching mode of the carboxylate group in EXP3174 in the ξ-crystal form, where the "bidentate" and "bridging" forms of COO^-/Ca^{2+} are shown in equal amounts in Figure S2 of SI. This

https://doi.org/10.1021/acsomega.4c07887
ACS Omega 2024, 9, 49683−49691

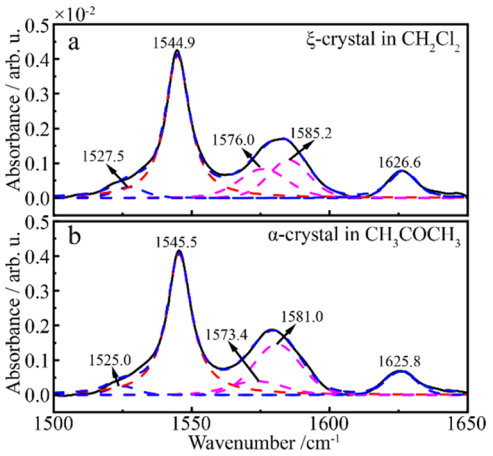

Figure 1. FTIR spectrum of S086 in the ξ-crystal form in CH_2Cl_2 (a) and the α-crystal form in acetone (b) in the spectral range of 1500−1650 cm^{-1}, with peak area normalized, and spectra fitted using Voigt functions. In particular, two asymmetric stretching modes of carboxylic groups in EXP3174 are estimated with an area ratio of 1:1 in (a) and 1:3 in (b). The strong and sharp peak is due to the asymmetric stretching mode of carboxylic acid, and the high-frequency peak is assigned to the amide-I mode in sacubitril.

yields an interesting link between the MicroED structure and IR spectral feature. Finally, the weak peak at 1525.0 cm^{-1} is due to the stretching mode of tetrazole.[50] In addition, a complete FTIR spectrum of the ξ-crystal form in CH_2Cl_2 and that of pure CH_2Cl_2 solvent are given at the end of SI.

Figure 1b shows an IR spectrum of the α-crystal form of S086 in acetone, which is also area-normalized in the spectral range 1500−1650 cm^{-1}. Clearly, the spectral feature of Figure 1b is quite similar to that of Figure 1a, indicating similar local structures of the two crystal forms in terms of the carboxylic acid and amide groups and their binding to Ca^{2+} ions. Based on this spectral similarity, we assign the 1545.5 cm^{-1} peak to the asymmetric stretching mode of carboxylic acid in sacubitril. We also tentatively assign the broad peak around 1560−1600 cm^{-1} to the *as*-mode of carboxylic acid in EXP3174. However, as shown in fitting, the two peaks are obtained at 1573.4 and 1581.0 cm^{-1} with an area ratio of 1:3, such a ratio is further supported by fitting the corresponding 2D IR diagonal peaks (see Figure S4 of SI). In addition, a complete FTIR spectrum of the α-crystal form in acetone and that of the acetone solvent are given at the end of SI.

3.2. How Carboxyl Group Interacts with Ca^{2+}.

Generally, ionic state of the carboxyl group may interact with metal cations in four types: unidentate, bridging, bidentate, and bridging-bidentate,[42] which are illustrated in Figure 2. Here, we term the last form as "trident." Interestingly, the asymmetric stretching (*as*) and symmetric stretching (*ss*) vibrational frequencies (υ_{as} and υ_{ss}) of the COO^- group were found to be highly dependent on the cation-binding state of the COO^- group. In particular, the frequency difference ($\Delta\upsilon_{a\text{-}s} = \upsilon_{as} - \upsilon_{ss}$) was found from solid acetate salts to be in the order of

$$\Delta\nu_{a\text{-}s}\ (\text{unidentate}) > \Delta\nu_{a\text{-}s}\ (\text{ionic}) \approx \Delta\nu_{a\text{-}s}\ (\text{bridging}) > \Delta\nu_{a\text{-}s}\ (\text{bidentate}) \quad (1)$$

To examine the solvent effect on the above derived order of $\Delta\upsilon_{a\text{-}s}$, deuterated acetic acid (CD_3COO^-) and its interaction with calcium ions in various cases are examined at different binding geometries in dichloromethane (CH_2Cl_2) and dimethyl sulfoxide (DMSO), respectively, using implicit PCM solvent. The results are shown in Figure 3 and Table

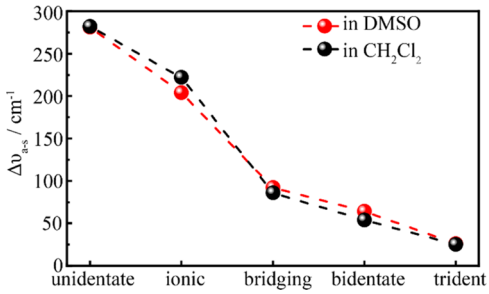

Figure 3. Calculated frequency separation between the asymmetric and symmetric COO^- stretching frequencies for the deuterated acetic acid (CD_3COO^-) in dichloromethane (CH_2Cl_2, black) and dimethyl sulfoxide (DMSO, red) solutions with calcium ions to form the "unidentate," "bridging," "bidentate," and "trident" structures, in comparison to that of the "ionic" form.

S1 of SI. As can be seen from Figure 3, in both solvents, we have

$$\Delta\upsilon_{a\text{-}s\ (\text{unidentate})} > \Delta\upsilon_{a\text{-}s\ (\text{ionic})} > \Delta\upsilon_{a\text{-}s\ (\text{bridging})} > \Delta\upsilon_{a\text{-}s\ (\text{bidentate})} > \Delta\upsilon_{a\text{-}s\ (\text{trident})} \quad (2)$$

where the order $\Delta\upsilon_{a\text{-}s\ (\text{ionic})}$ is predicted to be significantly larger than $\Delta\upsilon_{a\text{-}s\ (\text{bridging})}$. This differs from that reported earlier in eq 1: $\Delta\upsilon_{a\text{-}s\ (\text{ionic})} \approx \Delta\upsilon_{a\text{-}s\ (\text{bridging})}$.[42] We believe this discrepancy may be related to different structural constraints in solid vs solution. To address this, bridging binding was examined by varying the C═O bond length and the OCO bond angle, knowing that the optimized "ionic" state in CH_2Cl_2 has the C═O bond length and the OCO bond angle optimized at 1.26 Å and 126.7°, respectively, whereas the "bridging" state has the C═O bond angle and the OCO bond angle optimized at 1.26 Å and 122.4°, respectively.

More specifically, we examined bond-angle and bond-length influences on the value of $\Delta\upsilon_{a\text{-}s\ (\text{bridging})}$, and the results are listed in Tables S2 and S3 of SI, respectively. As can be seen, by increasing the C═O bond length or by enlarging the OCO bond angle, the value of $\Delta\upsilon_{a\text{-}s\ (\text{bridging})}$ increases. In particular, when the OCO bond angle of the "bridging" state is ca. 3.3° larger than that of the "ionic" state, one obtains $\Delta\upsilon_{a\text{-}s\ (\text{ionic})} \approx$

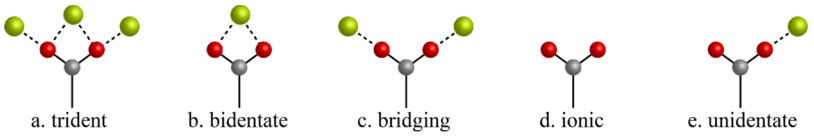

Figure 2. Illustration of a COO^- group and its binding with a calcium ion in different forms. The frequency difference between asymmetric and symmetric COO^- stretching vibration modes ($\Delta\upsilon_{a\text{-}s} = \upsilon_{as} - \upsilon_{ss}$) is in ascending order from left to right.

https://doi.org/10.1021/acsomega.4c07887
ACS Omega 2024, 9, 49683−49691

$\Delta\upsilon_{a\text{-}s\ (bridging)}$. It was also predicted earlier by Nara et al. that the frequency difference $\Delta\upsilon_{a\text{-}s}$ at the level of HF/6-31+G** depends on the C═O bond length and the OCO bond angle,[51] which agrees with our calculational results at the DFT level. Therefore, it is likely that for the bridging binding form, the C═O bond length or the OCO bond angle in the solid differs from those in the solution. This is further illustrated below for the ξ-form of the S086 crystal.

Our aim of this study is to examine the local structures of S086 in both ξ- and α-crystal forms suspended in organic solvent (Figure S1c of SI). Thermal analysis of the two crystals (thermogravimetry and differential scanning calorimetry) showed similar results (Figure S1d,e of SI), indicating that the two crystals have similar structures and cannot be differentiated in a straightforward way from their thermal behaviors.

Presumably, the local environment of carboxylic acid in S086 is comparable to that in the solid phase reported earlier[42] and is definitely more complex than CD_3COO^- in CH_2Cl_2 or DMSO. In the structure of the ξ-crystal of S086, the OCO bond angle of the "bridging" state of the carboxylic acid of EXP3174 is determined to be 125.1° from Figure S2c of SI, which is ca. 2.8° larger than that of the "ionic" state of the carboxylic acid of EXP3174 (122.3°). This suggests that in the ξ-crystal form, $\Delta\upsilon_{a\text{-}s\ (ionic)}$ is close to $\Delta\upsilon_{a\text{-}s\ (bridging)}$, which is consistent with the frequency-separation order predicted above for the solid sample.[42]

3.3. How Carboxyl Group Interacts with Ca^{2+} in S086.

Varying the binding geometry between the carboxylic groups and Ca^{2+} ions can lead to different asymmetric stretching vibration frequencies of multiple COO^- groups, which occurs in both sacubitril and EXP3174 in S086. This makes it possible to characterize relevant local structures of the drug–drug complex based on the frequency variations of the asymmetric stretching modes.

To decipher the structural origin of the vibration features of the multiple COO^- groups in S086, we first define an "ionic state" of S086, which is a mixture of sacubitril and EXP3174 at 1:1 molar ratio without adding calcium ion. Two solvents were used separately to dissolve the mixture, namely, CH_2Cl_2 and acetone. For the ionic state, we obtain the asymmetric and symmetric COO^- stretching frequency difference in each solvent and still term this value as $\Delta\upsilon_{a\text{-}s\ (ionic)}$ in the corresponding solvent. Similarly, for S086, we also obtain the asymmetric and symmetric COO^- stretching frequency differences for both sacubitril and EXP3174 in each solvent and term these values as $\Delta\upsilon_{a\text{-}s\ (sample)}$ in the corresponding solvent for a specific molecule (sacubitril or EXP3174). To measure the asymmetric and symmetric COO^- stretching vibration frequencies of sacubitril and EXP3174, samples in various solvent conditions and powdered forms and also in the KBr matrix were used. The IR spectra are given in Figures S5–S11 of SI. We then calculate the value of $\Delta\upsilon_{a\text{-}s\ (sample)} - \Delta\upsilon_{a\text{-}s\ (ionic)}$ for each molecule in the desired solvent. The results are listed in Figure 4. Based on the order of the frequency difference described in eq 1, we obtain the binding type for the carboxylate anions in sacubitril and EXP3174 in both ξ- and α-crystal forms.

3.3.1. Local Structure of EXP3174. We first examined the case of EXP3174. As shown in Figure 1a,b, both ξ- and α-crystal forms of S086 have two asymmetric stretching modes (υ_{as} = 1576.0 and 1585.2 cm^{-1} for the former and 1573.4 and 1581.0 cm^{-1} for the latter, with values listed in Tables S5 and S6 of SI), indicating two different COO^- local structures in each crystal. The binding geometries of these two different COO^- groups to Ca^{2+} ion are shown in Figure 4a for the ξ-crystal form and Figure 4b for the α-crystal form, by comparing the value of $\Delta\upsilon_{a\text{-}s\ (sample)} - \Delta\upsilon_{a\text{-}s\ (ionic)}$.

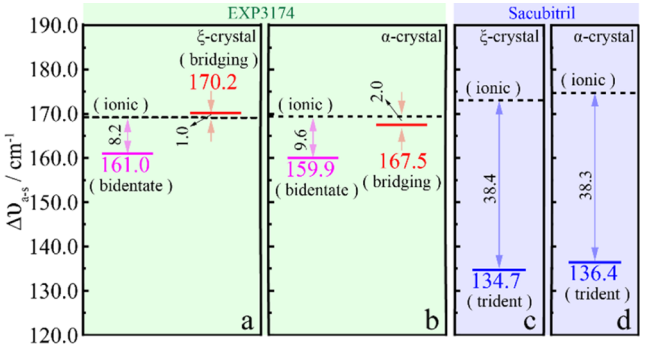

Figure 4. Asymmetric and symmetric COO^- vibrational frequency difference analysis. $\Delta\upsilon_{a\text{-}s\ (ionic)}$ (black dashed lines) were obtained from EXP3174: sacubitril = 1:1 (without Ca^{2+}) in CH_2Cl_2 (a and c) or in acetone (b and d), and $\Delta\upsilon_{a\text{-}s\ (sample)}$ (colored solid lines) were obtained from S086 in the ξ-crystal form in CH_2Cl_2 (a and c) and the α-crystal form in acetone (b and d). Pink lines: derived from the low-frequency *as*-COO^- modes of EXP3174; red solid lines: derived from the high-frequency *as*-COO^- modes of EXP3174; blue solid lines: derived from the *as*-COO^- modes of sacubitril. Arrows show the values of $[\Delta\upsilon_{a\text{-}s\ (sample)} - \Delta\upsilon_{a\text{-}s\ (ionic)}]$. Data were summarized in Tables S5 and S6 of SI. See the text for details.

For the ξ-crystal form (Figure 4a), $\Delta\upsilon_{a\text{-}s\ (ionic)}$ is shown by a black dashed line (169.2 cm^{-1}, see Table S5 of SI), and $\Delta\upsilon_{a\text{-}s\ (sample)}$ value is shown by a pink line (161.0 cm^{-1}, see Table S5) for the lower-frequency *as*-component (with υ_{as} = 1576.0 cm^{-1}), and that is shown by a red line (170.2 cm^{-1}, see Table S5) for the higher-frequency *as*-component (with υ_{as} = 1585.2 cm^{-1}). Here, the value of $\Delta\upsilon_{a\text{-}s\ (ionic)}$ = 169.2 cm^{-1}, agrees with the value of the ionic state reported earlier.[42] The low-frequency *as*-mode with $\Delta\upsilon_{a\text{-}s\ (sample)}$ = 161.0 cm^{-1} can be assigned to a "bidentate" bound COO^-, by comparing its $[\Delta\upsilon_{a\text{-}s\ (sample)} - \Delta\upsilon_{a\text{-}s\ (ionic)}]$ value (8.2 cm^{-1}) to the result reported by Nara et al.[52] in parvalbumin where Glu62 and Glu100 each formed a bidentate binding with Ca^{2+} with $\Delta\upsilon_{a\text{-}s\ (sample)} - \Delta\upsilon_{a\text{-}s\ (ionic)}$ = 14.0 cm^{-1}. On the other hand, the high-frequency *as*-mode with $\Delta\upsilon_{a\text{-}s\ (sample)}$ = 170.2 cm^{-1} can be assigned to a "bridging" bound COO^- since its $[\Delta\upsilon_{a\text{-}s\ (sample)} - \Delta\upsilon_{a\text{-}s\ (ionic)}]$ value is quite small, which agrees with the order of $\Delta\upsilon_{a\text{-}s\ (ionic)} \approx \Delta\upsilon_{a\text{-}s\ (bridging)}$ shown in eq 1. Here, Figure 4a shows that bridging COO^- has a larger $\Delta\upsilon_{a\text{-}s}$ value than bidentate COO^-, which also obeys the frequency-difference order shown in eq 1.

As shown in Figure 1a and its fitting results listed in Table S4 of SI, the two *as*-COO^- modes of EXP3174 (υ_{as} = 1576.0 and 1585.2 cm^{-1}) have an area ratio close to 1:1, we thus conclude from the IR results that in the unit cell of the ξ-crystal form, "bidentate" and "bridging" COO^- have a molar ratio of 1:1. This is proposed and is illustrated in Figure 5a. Such results indeed agree with the crystal structure shown in Figure S2 of SI in which two "bidentate" and two "bridging" COO^- of EXP3174 can be seen in the ξ-crystal form of S086. Therefore, we establish a connection between the IR spectra of the COO^- groups and its local structure in the ξ-form of S086.

Based on the same analogy, IR data analysis was carried out for the α-crystal form of S086 and the results are shown in

https://doi.org/10.1021/acsomega.4c07887
ACS Omega 2024, 9, 49683−49691

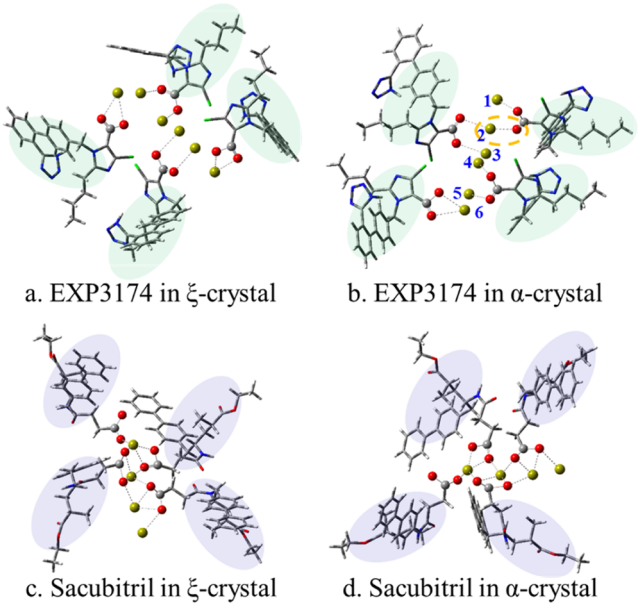

Figure 5. Illustration of local structures in the ξ-crystal form (a and c) and the α-crystal form (b and d) of S086 deduced from the vibrational frequency analysis of the carboxyl groups of EXP3174 (upper row) and sacubitril (lower row). Six Ca^{2+} ions are numbered in (b). Internal water molecules are ignored for simplification in (a) and are unknown in (b).

Figure 4b; we assign the low-frequency *as*-COO^- mode at 1573.4 cm^{-1} for the EXP3174 molecule (Figure 1b) to a "bidentate" binding to Ca^{2+}, and the corresponding high-frequency mode at 1581.0 cm^{-1} to a "bridging" binding to Ca^{2+}, and the molar ratio of these two types of COO^- groups is found to be 1:3 (Table S4 of SI). The local structure of COO^- in the α-crystal form of S086 is proposed in Figure 5b.

In the ξ-crystal form (Figure S2a), two EXP3174 molecules form "bidentate" binding with Ca^{2+}, locating on the two outer sides of the unit cell, respectively, while the other two EXP3174 form "bridging" binding with Ca^{2+}, situating on the middle of the unit cell and being adjacent to each other. This is illustrated in Figure 5a. Our analysis shows that in the α-crystal form, it is likely that one "bidentate" and three "bridging" COO^- groups exist in EXP3174 molecules.

The ξ-crystal form is prepared by altering the crystal structure of the α-crystal form under the influence of the solvent dichloromethane, and the two are found to have similar FTIR spectra in the COO^- stretching and amide-I mode vibration frequency region (Figure 1). Therefore, we speculate that one "bidentate" binding in the α-crystal form is located near the edge of its unit cell, which is similar to that in the ξ-crystal form, whereas the other three "bridging" bindings are arranged sequentially from inside of the unit cell to outside, and the two neighboring COO^- groups on the outside share the same Ca^{2+}. This is illustrated in Figure 5b.

Thus, compared with the α-crystal form, the relative position and connection between two types of coordinate COO^- in EXP3174 of the ξ-crystal form are different. During the process of crystal transformation, we hypothesize that the ligand bond between the outermost "bridging" COO^- in the α-crystal form and Ca^{2+} No. 2 (Figure 5b) breaks under the action of dichloromethane (as shown in orange dashed circle in Figure 5b) and forms a new ligand bond with the Ca^{2+} No. 1, which ultimately becomes two "bridging" and two "bidentate" COO^- groups (the ξ-crystal form).

3.3.2. Local Structure of Sacubitril. As shown in Figure 1ab, there is only one type of *as*-COO^- mode in sacubitril of each crystal form (υ_{as} = 1544.9 cm^{-1} for the ξ-crystal form and υ_{as} = 1545.5 cm^{-1} for the α-crystal form). Figure 4c shows $\Delta\upsilon_{a\text{-}s\ (ionic)}$ for the ionic state of S086 (173.1 cm^{-1}, black dashed line) and $\Delta\upsilon_{a\text{-}s\ (sample)}$ for the ξ-crystal form of S086 (134.7 cm^{-1}, blue solid line), which are obtained from the FTIR spectra of corresponding samples in CH_2Cl_2. Their difference (38.4 cm^{-1}) is much larger than those of "bidentate" (8.2 cm^{-1}) and "bridging" (1.0 cm^{-1}) of EXP3174 shown in Figure 4a, suggesting a "trident" binding between COO^- and Ca^{2+} for sacubitril in this crystal form. Indeed, the crystal structure (Figure S2 of SI) shows that four COO^- groups are in "trident" coordination with four Ca^{2+}. Such a local binding structure is demonstrated in Figure 5c.

Similarly, Figure 4d shows $\Delta\upsilon_{a\text{-}s\ (ionic)}$ for the ionic state of S086 (174.7 cm^{-1}, black dashed line) and $\Delta\upsilon_{a\text{-}s\ (sample)}$ for the α-crystal form of S086 (136.4 cm^{-1}, blue solid line), which are measured from the FTIR spectra of corresponding samples in acetone. Their difference (38.3 cm^{-1}) is much larger than those of "bidentate" (9.6 cm^{-1}) and "bridging" (2.0 cm^{-1}) of EXP3174 shown in Figure 4b and is close to that of the "trident" binding in the ξ-crystal form (38.4 cm^{-1}, Figure 4c), therefore also suggesting a "trident" binding between the COO^- group and Ca^{2+} for sacubitril in the α-crystal form. Such a deduced local binding structure is illustrated in Figure 5c for the α-crystal form of S086.

In addition, as shown in Figure S5, EXP3174 monomer in acetone shows an *as*-COO^- mode at 1581.2 cm^{-1}, whereas EXP3174 in the α-crystal in the same solvent shows a double *as*-COO^- mode at 1573.4 and 1581.0 cm^{-1}. This indicates the influence of Ca^{2+} on EXP3174 in the α-crystal: two types of binding between the COO^- group and Ca^{2+} ion exist. Quite differently for sacubitril, as shown in Figure S6, its monomer in acetone shows an *as*-COO^- mode at 1581.0 cm^{-1}, which is similar to that of EXP3174. However, in the α-crystal in the same solvent, only a significantly red-shifted *as*-COO^- mode is shown at 1545.5 cm^{-1}. This indicates the influence of Ca^{2+} on sacubitril in the α-crystal: a tighter binding, with respect to that of EXP3174, between the COO^- group and Ca^{2+} exists for sacubitril.

4. CONCLUSIONS

In summary, since the ξ-crystal form of S086 is recrystallized from the α-crystal form in CH_2Cl_2, they bear certain structural similarities. Based on the results presented above and assuming the two crystals have the same molecular composition (Scheme 1), it is believed that four EXP3174 molecules in the α-crystal form can be classified into two types: three have "bridging" type of the COO^- groups binding to Ca^{2+} ions and one has "bidentate" type of COO^- group binding to Ca^{2+} ions, while in ξ-crystal form, the ratio of "bridging" and "bidentate" types of the COO^- groups is 1:1. On the other hand, in both crystals, four sacubitril molecules are believed to have "trident" type of COO^- groups binding to Ca^{2+} ions. It is therefore concluded that the COO^- groups of EXP3174 have undergone local environment change in the process of recrystallization from the α- to ξ-crystal, which is why similar molecular moieties can form two different crystal structures.

Through this study, we established a connection between the IR absorption profile of metal cation ligands and the

https://doi.org/10.1021/acsomega.4c07887
ACS Omega 2024, 9, 49683−49691

MicroED-determined molecular structure. Particularly, the asymmetric and symmetric stretching modes of the carboxyl groups of both sacubitril and EXP3174 were utilized. Nonlinear 2D IR spectroscopy was used to reveal intramolecularly coupled vibration modes, which was used to differentiate the asymmetric stretching modes of sacubitril from those of EXP3174 in the core region of the local structures. Our study demonstrates the importance of linear and nonlinear IR spectroscopy in illustrating local structural details in drug cocrystals.

■ ASSOCIATED CONTENT

Supporting Information

The Supporting Information is available free of charge at https://pubs.acs.org/doi/10.1021/acsomega.4c07887.

S086 samples in suspensions, XRD spectra, ξ-crystal structure determined by MicroED, vibrational frequency analysis, 2D IR spectra of the two crystal forms and their analysis, and associated linear IR spectral results (PDF)

■ AUTHOR INFORMATION

Corresponding Author

Jianping Wang − *Beijing National Laboratory for Molecular Sciences, Molecular Reaction Dynamics Laboratory, CAS Research/Education Center for Excellence in Molecular Sciences, Institute of Chemistry, Chinese Academy of Sciences, Beijing 100190, P. R. China; University of Chinese Academy of Sciences, Beijing 100049, P. R. China;* orcid.org/0000-0001-7127-869X; Phone: (+86)-010-62656806; Email: jwang@iccas.ac.cn; Fax: (+86)-010-62563167

Authors

Wenjie Xu − *Shenzhen Salubris Pharmaceutical Co., Ltd., Shenzhen, Guangdong 518118, P. R. China*

Haiyan Xu − *Beijing National Laboratory for Molecular Sciences, Molecular Reaction Dynamics Laboratory, CAS Research/Education Center for Excellence in Molecular Sciences, Institute of Chemistry, Chinese Academy of Sciences, Beijing 100190, P. R. China; University of Chinese Academy of Sciences, Beijing 100049, P. R. China*

Jie Yan − *Shenzhen Salubris Pharmaceutical Co., Ltd., Shenzhen, Guangdong 518118, P. R. China*

Song Li − *Shenzhen Salubris Pharmaceutical Co., Ltd., Shenzhen, Guangdong 518118, P. R. China*

Pengyun Yu − *Beijing National Laboratory for Molecular Sciences, Molecular Reaction Dynamics Laboratory, CAS Research/Education Center for Excellence in Molecular Sciences, Institute of Chemistry, Chinese Academy of Sciences, Beijing 100190, P. R. China; University of Chinese Academy of Sciences, Beijing 100049, P. R. China;* Present Address: Hefei National Laboratory for Physical Sciences at the Microscale, University of Science and Technology of China, Hefei 230026, China

Juan Zhao − *Beijing National Laboratory for Molecular Sciences, Molecular Reaction Dynamics Laboratory, CAS Research/Education Center for Excellence in Molecular Sciences, Institute of Chemistry, Chinese Academy of Sciences, Beijing 100190, P. R. China; University of Chinese Academy of Sciences, Beijing 100049, P. R. China*

Fan Yang − *Beijing National Laboratory for Molecular Sciences, Molecular Reaction Dynamics Laboratory, CAS Research/Education Center for Excellence in Molecular Sciences, Institute of Chemistry, Chinese Academy of Sciences, Beijing 100190, P. R. China; University of Chinese Academy of Sciences, Beijing 100049, P. R. China*

Complete contact information is available at: https://pubs.acs.org/10.1021/acsomega.4c07887

Author Contributions

[‖]W.X. and H.X. contributed equally.

Notes

The authors declare no competing financial interest.

■ ACKNOWLEDGMENTS

Financial support from the National Natural Science Foundation of China (Grant Nos. 21973102 and 21327802) and the Shenzhen Science and Technology Program (Grant No. KQTD20200820151701004) is acknowledged.

■ REFERENCES

(1) Irigoyen, M.-C.; De Angelis, K.; dos Santos, F.; Dartora, D. R.; Rodrigues, B.; Consolim-Colombo, F. M. Hypertension, Blood Pressure Variability, and Target Organ Lesion. *Curr. Hypertens. Rep.* **2016**, *18* (4), 1−13.

(2) Poulter, N. R.; Prabhakaran, D.; Caulfield, M. Hypertension. *Lancet* **2015**, *386* (9995), 801−812.

(3) Xiao, Y.; Zhou, Z.; Sun, J.; Xing, W.; Yan, J.; Xu, W.; Lu, Y.; Liu, T.; Jin, Y. Protective effect of novel angiotensin receptor neprilysin inhibitor S086 on target organ injury in spontaneously hypertensive rats. *Biomed. Pharmacother.* **2024**, *170*, 1−12.

(4) Kou, M.; Wang, X.; Ma, H.; Li, X.; Heianza, Y.; Qi, L. Degree of Joint Risk Factor Control and Incident Heart Failure in Hypertensive Patients. *JACC-Heart Fail.* **2023**, *11* (6), 678−688.

(5) Yusuf, S. Effect of Enalapril on Survival in Patients with Reduced Left Ventricular Ejection Fractions and Congestive Heart Failure. *New Engl. J. Med.* **1991**, *325* (5), 293−302.

(6) Wang, Y.; Zhou, R.; Lu, C.; Chen, Q.; Xu, T.; Li, D. Effects of the Angiotensin-Receptor Neprilysin Inhibitor on Cardiac Reverse Remodeling: Meta-Analysis. *J. Am. Heart Assoc.* **2019**, *8* (13), 1−10.

(7) Burnier, M.; Brunner, H. R. Angiotensin II receptor antagonists in hypertension. *Kidney Int.* **1998**, *54*, S107−S111.

(8) Michel, M. C.; Brunner, H. R.; Foster, C.; Huo, Y. Angiotensin II type 1 receptor antagonists in animal models of vascular, cardiac, metabolic and renal disease. *Pharmacol. Ther.* **2016**, *164*, 1−81.

(9) Bozkurt, B.; Nair, A. P.; Misra, A.; Scott, C. Z.; Mahar, J. H.; Fedson, S. Neprilysin Inhibitors in Heart Failure The Science, Mechanism of Action, Clinical Studies, and Unanswered Questions. *JACC-Basic Transl. Sci.* **2023**, *8* (1), 88−105.

(10) Kang, G.; Banerjee, D. Neprilysin Inhibitors in Cardiovascular Disease. *Curr. Cardiol. Rep.* **2017**, *19* (2), 1−7.

(11) McMurray, J. J. V.; Packer, M.; Desai, A. S.; Gong, J.; Lefkowitz, M. P.; Rizkala, A. R.; Rouleau, J. L.; Shi, V. C.; Solomon, S. D.; Swedberg, K.; Zile, M. R. Angiotensin-Neprilysin Inhibition versus Enalapril in Heart Failure. *New Engl. J. Med.* **2014**, *371* (11), 993−1004.

(12) Chen, Y.; He, Q.; Mo, D.; Chen, L.; Lu, J.; Li, R.; Huang, J. The angiotensin receptor and neprilysin inhibitor, LCZ696, in heart failure: A meta-analysis of randomized controlled trials. *Medicine* **2022**, *101* (41), 1−6.

(13) Ruilope, L. M.; Dukat, A.; Boehm, M.; Lacourciere, Y.; Gong, J.; Lefkowitz, M. P. Blood-pressure reduction with LCZ696, a novel dual-acting inhibitor of the angiotensin II receptor and neprilysin: a randomised, double-blind, placebo-controlled, active comparator study. *Lancet* **2010**, *375* (9722), 1255−1266.

(14) Solomon, S. D.; Zile, M.; Pieske, B.; Voors, A. A.; Shah, A.; Kraigher-Krainer, E.; Shi, V.; Bransford, T.; Takeuchi, M.; Gong, J.; Lefkowitz, M.; Packer, M.; McMurray, J. J. V. The angiotensin receptor neprilysin inhibitor LCZ696 in heart failure with preserved

ejection fraction: a phase 2 double-blind randomised controlled trial. *Lancet* **2012**, *380* (9851), 1387−1395.
(15) China Hypertension Prevention Guidelines Revision Committee; Hypertension Alliance (China); China Association for the Promotion of International Exchange of Medical Care Hypertension Branch; Hypertension Branch of Chinese Geriatric Society; Hypertension Branch of Chinese Geriatric Health Care Association; Chinese Stroke Society and Chinese Center for Disease Control and Prevention Center for Chronic Noncommunicable Diseases. Chinese Guidelines for the Prevention and Treatment of Hypertension (2024 revision). *Zhonghua Gaoxueya Zazhi* **2024**, *32* (07), 603−700.
(16) Mancia, G.; Kreutz, R.; Brunström, M.; Burnier, M.; Grassi, G.; Januszewicz, A.; Muiesan, M. L.; Tsioufis, K.; Agabiti-Rosei, E.; Algharably, E. A. E.; Azizi, M.; Benetos, A.; Borghi, C.; Hitij, J. B.; Cifkova, R.; Coca, A.; Cornelissen, V.; Cruickshank, J. K.; Cunha, P. G.; Danser, A. H. J.; Pinho, R. M. d.; Delles, C.; Dominiczak, A. F.; Dorobantu, M.; Doumas, M.; Fernández-Alfonso, M. S.; Halimi, J.-M.; Járai, Z.; Jelaković, B.; Jordan, J.; Kuznetsova, T.; Laurent, S.; Lovic, D.; Lurbe, E.; Mahfoud, F.; Manolis, A.; Miglinas, M.; Narkiewicz, K.; Niiranen, T.; Palatini, P.; Parati, G.; Pathak, A.; Persu, A.; Polonia, J.; Redon, J.; Sarafidis, P.; Schmieder, R.; Spronck, B.; Stabouli, S.; Stergiou, G.; Taddei, S.; Thomopoulos, C.; Tomaszewski, M.; Van de Borne, P.; Wanner, C.; Weber, T.; Williams, B.; Zhang, Z.-Y.; Kjeldsen, S. E. 2023 ESH Guidelines for the management of arterial hypertension The Task Force for the management of arterial hypertension of the European Society of Hypertension: Endorsed by the International Society of Hypertension (ISH) and the European Renal Association (ERA): Erratum. *J. Hypertens.* **2024**, *42* (1), 194.
(17) An, J. New Sakubitri Calcium/valsartan Co-Amorphous. Korea, KR102149125B12020.
(18) Ksander, G. M.; Ghai, R. D.; Dejesus, R.; Diefenbacher, C. G.; Yuan, A.; Berry, C.; Sakane, Y.; Trapani, A. Dicarboxylic Acid Dipeptide Neutral Endopeptidase Inhibitors. *J. Med. Chem.* **1995**, *38* (10), 1689−1700.
(19) Schiering, N.; D'Arcy, A.; Villard, F.; Ramage, P.; Logel, C.; Cumin, F.; Ksander, G. M.; Wiesmann, C.; Karki, R. G.; Mogi, M. Structure of neprilysin in complex with the active metabolite of sacubitril. *Sci. Rep.* **2016**, *6*, No. 27909.
(20) Sachinidis, A.; Ko, Y.; Weisser, P.; zu Brickwedde, M.-k. M.; Düsing, R.; Christian, R.; Wieczorek, A. J.; Vetter, H. EXP3174, a metabolite of losartan (MK954, DuP753) is more potent than losartan in blocking the angiotensin ll-induced responses in vascular smooth muscle cells. *J. Hypertens.* **1993**, *11* (2), 155−162.
(21) Sun, J.; Xiao, Y.; Xu, W.; Xing, W.; Du, F.; Tian, M.; Xu, D.; Ren, Y.; Fang, X. Anti-hypertensive effect of a novel angiotensin II receptor neprilysin inhibitor (ARNi)-S086 in DSS rat model. *Front. Cardiovasc. Med.* **2024**, *11*, 1−12.
(22) Sun, J.; Xu, W.; Hua, H.; Xiao, Y.; Chen, X.; Gao, Z.; Li, S.; Jing, X.; Du, F.; Sun, G. Original Pharmacodynamic and pharmacokinetic effects of S086, a novel angiotensin receptor neprilysin inhibitor. *Biomed. Pharmacother.* **2020**, *129*, 1−10.
(23) Banerjee, M.; Nimkar, K.; Naik, S.; Patravale, V. Unlocking the potential of drug-drug cocrystals-A comprehensive review. *J. Controlled Release* **2022**, *348*, 456−469.
(24) Yan, J.; Xu, W.; Li, S.; Zheng, Y.; Zhi, J. Angiotensin II receptor antagonist metabolite and nep inhbitor composite, and preparation method thereof. China, CN108473474A2018.
(25) Yan, J.; Xu, W.; Li, S.; Tan, D. New crystal form of ARNi compound, preparation method therefor, and use thereof. China, CN118176190A2024.
(26) Wang, J.; Dai, X.-L.; Lu, T.-B.; Chen, J.-M. Temozolomide-Hesperetin Drug-Drug Cocrystal with Optimized Performance in Stability, Dissolution, and Tabletability. *Cryst. Growth Des.* **2021**, *21* (2), 838−846.
(27) Saikia, B.; Sultana, N.; Kaushik, T.; Sarma, B. Engineering a Remedy to Improve Phase Stability of Famotidine under Physiological pH Environments. *Cryst. Growth Des.* **2019**, *19* (11), 6472−6481.
(28) Wang, L.; Li, S.; Xu, X.; Xu, X.; Wang, Q.; Li, D.; Zhang, H. Drug-drug cocrystals of theophylline with quercetin. *J. Drug Delivery Sci. Technol.* **2022**, *70*, 1−9.
(29) Ul Islam, N.; Khan, E.; Umar, M. N.; Shah, A.; Zahoor, M.; Ullah, R.; Bari, A. Enhancing Dissolution Rate and Antibacterial Efficiency of Azithromycin through Drug-Drug Cocrystals with Paracetamol. *Antibiotics* **2021**, *10* (8), 1−16.
(30) Xu, H.; Tang, Y.; Wu, Q.; Li, W.; Zhou, L.; Wang, M.; Zou, F. J. J. o. M. S. A drug−drug cocrystal strategy to regulate stability and solubility: A case study of Temozolomide/caffeic acid. *J. Mol. Struct.* **2024**, *1312*, 1−10.
(31) Yin, H.-M.; Xie, J.-Y.; Jiang, J.-Y.; Hong, M.; Zhu, B.; Ren, G.-B.; Qi, M.-H. Strategy to Tune the Performance of Two Drug Components: Drug-Drug Cocrystals of Lobaplatin with Flavonoids. *Cryst. Growth Des.* **2022**, *22* (4), 2602−2610.
(32) Dong, T.; Yu, P.; Zhao, J.; Wang, J. Site specifically probing the unfolding process of human telomere i-motif DNA using vibrationally enhanced alkynyl stretch. *Phys. Chem. Chem. Phys.* **2024**, *26* (5), 3857−3868.
(33) Shi, L.; Yu, P.; Zhao, J.; Wang, J. Ultrafast Intermolecular Vibrational Energy Transfer in Hexahydro-1,3,5-trinitro-1,3,5-triazine in Molecular Crystal by 2D IR Spectroscopy. *J. Phys. Chem. C* **2020**, *124* (4), 2388−2398.
(34) Rosenfeld, D. E.; Gengeliczki, Z.; Smith, B. J.; Stack, T. D. P.; Fayer, M. D. Structural Dynamics of a Catalytic Monolayer Probed by Ultrafast 2D IR Vibrational Echoes. *Science* **2011**, *334* (6056), 634−639.
(35) Cho, M. Coherent two-dimensional optical spectroscopy. *Chem. Rev.* **2008**, *108* (4), 1331−1418.
(36) Wang, J. Ultrafast two-dimensional infrared spectroscopy for molecular structures and dynamics with expanding wavelength range and increasing sensitivities: from experimental and computational perspectives. *Int. Rev. Phys. Chem.* **2017**, *36* (3), 377−431.
(37) Bredenbeck, J.; Helbing, J.; Nienhaus, K.; Nienhaus, G. U.; Hamm, P. Protein ligand migration mapped by nonequilibrium 2D-IR exchange spectroscopy. *Proc. Natl. Acad. Sci. U.S.A.* **2007**, *104* (36), 14243−14248.
(38) Kratochvil, H. T.; Carr, J. K.; Matulef, K.; Annen, A. W.; Li, H.; Maj, M.; Ostmeyer, J.; Serrano, A. L.; Raghuraman, H.; Moran, S. D.; Skinner, J. L.; Perozo, E.; Roux, B.; Valiyaveetil, F. I.; Zanni, M. T. Instantaneous ion configurations in the K^+ ion channel selectivity filter revealed by 2D IR spectroscopy. *Science* **2016**, *353* (6303), 1040−1044.
(39) Zhao, Y.; Yu, P.; Wang, J. Chlorine-Modified Soluble Melem-Based Graphitic Carbon Nitrite: Facile Synthesis, Catalytic Property and Ultrafast 2D IR Spectroscopic Characterization. *ChemPhysChem* **2024**, *25*, No. e202400356.
(40) Remorino, A.; Korendovych, I. V.; Wu, Y. B.; DeGrado, W. F.; Hochstrasser, R. M. Residue-Specific Vibrational Echoes Yield 3D Structures of a Transmembrane Helix Dimer. *Science* **2011**, *332* (6034), 1206−1209.
(41) Nakamoto, K. *Infrared and Raman Spectra of Inorganic and Coordination Compounds*, 6th ed.; John Wiley & Sons, Inc.: Hoboken, NJ, 1986; pp 1−413.
(42) Deacon, G. B.; Phillips, R. J. Relationships between the carbon-oxygen stretching frequencies of carboxylato complexes and the type of carboxylate coordination. *Coord. Chem. Rev.* **1980**, *33* (3), 227−250.
(43) Middleton, C. T.; Woys, A. M.; Mukherjee, S. S.; Zanni, M. T. Residue-specific structural kinetics of proteins through the union of isotope labeling, mid-IR pulse shaping, and coherent 2D IR spectroscopy. *Methods* **2010**, *52* (1), 12−22.
(44) Hamm, P.; Zanni, M. *Concepts and Methods of 2D Infrared Spectroscopy*, 6th ed.; Cambridge University Press: New York, 2011; pp 1−298.
(45) Frisch, M. J.; Trucks, G. W.; Schlegel, H. B.; Scuseria, G. E.; Robb, M. A.; Cheeseman, J. R.; Scalmani, G.; Barone, V.; Mennucci, B.; Petersson, G. A. *Gaussian 09*; A.02Gaussian, Inc: Pittsburgh, PA, 2009; pp 1−121.

https://doi.org/10.1021/acsomega.4c07887
ACS Omega 2024, 9, 49683−49691

(46) Almerindo, G. I.; Tondo, D. W.; Pliego, J. R., Jr Ionization of organic acids in dimethyl sulfoxide solution:: A theoretical ab initio calculation of the pKa using a new parametrization of the polarizable continuum model. *J. Phys. Chem. A* **2004**, *108* (1), 166−171.
(47) Lu, S. I.; Chiu, C.; Wang, Y. Density functional theory calculations of dynamic first hyperpolarizabilities for organic molecules in organic solvent: Comparison to experiment. *J. Chem. Phys.* **2011**, *135* (13), 1−7.
(48) Majumdar, D.; Das, D.; Sreejith, S. S.; Das, S.; Biswas, J. K.; Mondal, M.; Ghosh, D.; Bankura, K.; Mishra, D. Dicyanamide-interlaced assembly of Zn(II)-schiff-base complexes derived from salicylaldimino type compartmental ligands: Syntheses, crystal structures, FMO, ESP, TD-DFT, fluorescence lifetime, in vitro antibacterial and anti-biofilm properties. *Inorg. Chim. Acta* **2019**, *489*, 244−254.
(49) Duczmal, K.; Darowska, M.; Raczynska, E. D. Spectral (DFT-IR, FT-IR and UV) similarities and differences between substrate (pyruvate) and inhibitor (oxamate) of lactic dehydrogenase (LDH). *Vib. Spectrosc.* **2005**, *37* (1), 77−82.
(50) Gao, D.; Tang, X.; Wang, X.; Yang, X.; Zhang, P.; Che, G.; Han, J.; Hattori, T.; Wang, Y.; Dong, X.; Zheng, H.; Li, K.; Mao, H.-k. Phase transition and chemical reactivity of 1H-tetrazole under high pressure up to 100 GPa. *Phys. Chem. Chem. Phys.* **2021**, *23* (35), 19503−19510.
(51) Nara, M.; Torii, H.; Tasumi, M. Correlation between the vibrational frequencies of the carboxylate group and the types of its coordination to a metal ion: An ab initio molecular orbital study. *J. Phys. Chem. A* **1996**, *100* (51), 19812−19817.
(52) Nara, M.; Morii, H.; Tanokura, M. Coordination to divalent cations by calcium-binding proteins studied by FTIR spectroscopy. *Biochim. Biophys. Acta-Biomembr.* **2013**, *1828* (10), 2319−2327.

https://doi.org/10.1021/acsomega.4c07887
ACS Omega 2024, 9, 49683−49691